Supplemental Material Captions

Supplemental Table S1. Summary of rhythmic and non-rhythmic parameters by ROI and mouse. All ROIs analyzed for this study across 4 mice are arrayed in rows. Checkmarks indicate the detection of statistically significant circadian rhythmicity (Cosinor fit p<0.05) for each of our major measures, for 48h DD and LD datasets. The final 2 columns list the # of rhythmic coherence relationships each ROI had with others from the same mouse. Note that for AVP10, a DD recording was incomplete and not included in the dataset. Discrete, unambiguous Ca^{2+} waves were less common in AVP63, so waves were not counted for rhythmicity for this mouse.

Supplemental Figure S1: Behavioral rhythmicity. All 4 mice recorded from for this study had Minimitter G2 emitters implanted. Robust rhythmicity of locomotor behavior was verified for each mouse prior to recordings. Shown here is an example of locomotor activity (Mouse AVP44) collected contemporaneously with the Ca^{2+} recordings used for analysis. Raw behavior actograms are shown for 48h DD, 48h LD. Below are the associated periodograms for each 48h recording.

Supplemental Figure S2: Circadian Rhythmicity in Duration of Dynamic Calcium Events of Individual AVP Neurons. A: Representative 5-minute calcium trace demonstrating analysis of duration of calcium waves (time between the green (onset) and red (offset) triangles). **B:** Heat maps illustrating the duration of calcium waves of individual AVP neurons (rows) by timepoint (columns) in both DD and LD. Neurons which exhibited significant circadian rhythms in calcium wave duration appear above the dashed line. Plotted beneath are the population averages and standard errors for each timepoint. For DD the population was arrhythmic according to cosinor, while in DD a rhythm was detected (p=0.013; cosine superimposed on histogram). **C:** Polar plots illustrating the phase distribution, and pie charts showing the proportion of AVP neurons/ROIs exhibiting significant circadian rhythms in calcium waves duration in both DD and LD. The direction of the bar represents hour in CT for DD or ZT for LD. The length of the bar represents number of ROIs. Mean phase ± SEM is indicated in green. **D:** Phenotype tracking plots indicating the stability/change in rhythm state of individual AVP ROIs between recording days (DD Day1-DD Day2) under constant darkness (left) and between lighting conditions (right). Red lines indicate a loss of rhythmicity between conditions, green lines a gain of rhythmicity, and blue lines indicate no change in rhythm state between conditions. Black triangles on the axes indicate the division between rhythmic (above) and arrhythmic (below) ROIs.

Supplemental Figure S3: Circadian Rhythmicity in Inter-event Interval of Dynamic Calcium Events of Individual AVP Neurons. A: Representative 5-minute calcium trace demonstrating analysis of calcium wave inter-event interval (time between the red (offset) triangle of one wave and the green (onset) triangles of the next wave). **B:** Heat maps illustrating the inter-event interval of calcium waves of individual AVP neurons (rows) by timepoint (columns) in both DD and LD. Neurons which exhibited significant circadian rhythms in inter-event interval of calcium waves appear above the dashed line and triangle. Plotted beneath are the population averages and standard errors for each timepoint. Population-level circadian rhythmicity was not observed for DD or LD (cosinor p> 0.05). **C:** Polar plots illustrating the phase distributions, and pie charts the proportion of AVP neurons/ROIs exhibiting significant circadian rhythms in inter-event interval of calcium waves in both DD and LD. The direction of the bar represents hour in CT for DD or ZT for LD. The length of the bar represents number of ROIs. Mean phase ± SEM is indicated in green. **D:** Phenotype tracking plots indicating the stability/change in rhythm state of individual AVP ROIs between recording days (DD Day 1-DD Day 2) under constant darkness (left) and between lighting conditions (right). Red lines indicate a loss of rhythmicity between conditions, green lines a gain of rhythmicity, and blue lines indicate no change in rhythm state between conditions. Black triangles on the axes indicate the division between rhythmic (above) and arrhythmic (below) ROIs.

Supplemental Figure S4: Additional single-day measures of rhythmicity. **A-F**: Phenotype tracking plots indicating the stability/change in rhythmic state of individual AVP ROIs (A-E), or pairwise correlated relationships (F) between recording days in a LD cycle (LD Day 1-LD Day 2). Red lines indicate a loss of rhythmicity between conditions, green lines a gain of rhythmicity, and blue lines indicate no change in rhythm state between conditions. Black triangles on the axes indicate the division between rhythmic (above) and arrhythmic (below) ROIs. **G-I**: Polar plots showing phase of rhythms in ROIs for individual days in the study across the 3 primary measures of single-cell rhythms.

Supplemental Figure S5: Additional single-day measures of rhythmicity. A-C: Single-day polar plots for correlations (A), wave duration (B) and wave inter-event interval (C). Same conventions as previous figures.

Supplemental Figure S6: Multimodal summary of rhythmicity across measures. A-B: Histograms showing how rhythmicity in various single-cell measures overlaps within ROIs in 48h constant darkness (A) and in a 48h LD cycle (B). Furthest to the right, the blue histograms indicate the fraction of total ROIs that were rhythmic in *at least* 1, 2 or all 3 major parameters. **C**: Histogram reporting the number of pairwise rhythmic correlations per ROI for 48hDD (C) and 48hLD(D) datasets. Note that some mouse recordings had more ROIs than others (See Table S1), making a higher number of rhythmic correlations possible.

Supplemental Figure S7: Bootstrapping Population Results for Equal Contributions by Animal. The number of fluorescent ROIs varied widely from animal to animal. To determine if equal contributions from each animal would yield significantly rhythmic population results similar to data presented for Correlations in Figure 4 and Intensity in Figure 2, a bootstrapping approach was conducted on the data (see Methods). Rows in each heatmap represent an average at each time point (columns) of a population of measurements from an average of an equal number of ROIs or cross-correlations chosen from each animal. Each bootstrap trial of population measurements was performed 100 times. For the correlation heatmap pictured, the random number of cross-correlations chosen per animal was 28. For the Intensity, Acute Events, and Calcium Waves heatmaps, the number of ROIs randomly chosen from each animal was 10.

Supplemental Table S2: **Summary of bootstrapping trial results**. For all variables we ran a bootstrapping simulation with 3 different sampling counts (a range from undersampled to oversampled; Column 5). Figure S7 represents heatmaps from just one of these counts, a subset of this Table data. The last column indicates the % of the 100 trials/rows of the heatmap for which a significant cosine fit in the circadian range was found. Above 50% would mean that a preponderance of the trials exhibited rhythmicity, indicating a stronger likelihood of population rhythmicity.

Summary of Circadian Rhythmicity

Mouse ID - ROI #	Intensity		Acute Events		Ca Wave #		# Rhythmic Correlations	
	DD	LD	DD	LD	DD	LD	DD	LD
AVP10-0	n/a		n/a		n/a		n/a	3
AVP10-1	n/a	✓	n/a		n/a		n/a	4
AVP10-2	n/a	✓	n/a	✓	n/a		n/a	5
AVP10-3	n/a	✓	n/a		n/a		n/a	5
AVP10-4	n/a		n/a		n/a		n/a	5
AVP10-5	n/a		n/a		n/a		n/a	4
AVP10-6	n/a		n/a		n/a	✓	n/a	6
AVP10-7	n/a		n/a		n/a		n/a	6
AVP24-0		✓		✓			5	5
AVP24-1			✓	✓			4	3
AVP24-2							6	2
AVP24-3		✓	✓	✓		✓	3	2
AVP24-4			✓			✓	3	2
AVP24-5				✓		✓	8	2
AVP24-6	✓		✓	✓			3	6
AVP24-7	✓	✓	✓			✓	6	2
AVP24-8		✓		✓			4	7
AVP24-9	✓	✓	✓	✓	✓		2	2
AVP24-10		✓	✓	✓	✓		4	2
AVP24-11							5	4
AVP24-12				✓	✓		3	6
AVP24-13	✓	✓	✓	✓	✓		2	4
AVP24-14			✓				0	4
AVP44-0		✓		✓			2	0
AVP44-1	✓	✓	✓				1	0
AVP44-2		✓					1	1
AVP44-3			✓	✓		✓	5	4
AVP44-4		✓				✓	1	1
AVP44-5			✓	✓	✓		5	1
AVP44-6				✓			1	0
AVP44-7		✓					0	0
AVP44-8		✓				✓	2	0
AVP44-9	✓	✓	✓			✓	0	2
AVP44-10		✓					2	1
AVP63-0					n/a	n/a	9	3
AVP63-1	✓		✓		n/a	n/a	10	7
AVP63-2					n/a	n/a	10	5
AVP63-3	✓				n/a	n/a	16	10
AVP63-4	✓				n/a	n/a	6	5
AVP63-5	✓				n/a	n/a	14	4
AVP63-6					n/a	n/a	14	6
AVP63-7		✓			n/a	n/a	10	4
AVP63-8					n/a	n/a	6	8
AVP63-9	✓	✓	✓		n/a	n/a	5	2
AVP63-10	✓	✓			n/a	n/a	7	5
AVP63-11	✓				n/a	n/a	12	11
AVP63-12					n/a	n/a	11	1
AVP63-13	✓			✓	n/a	n/a	2	0
AVP63-14	✓	✓			n/a	n/a	3	10
AVP63-15	✓				n/a	n/a	4	7
AVP63-16	✓		✓		n/a	n/a	9	0
AVP63-17	✓	✓			n/a	n/a	4	2
AVP63-18	✓			✓	n/a	n/a	9	1
AVP63-19	✓	✓	✓	✓	n/a	n/a	16	5
AVP63-20	✓	✓			n/a	n/a	16	7
AVP63-21	✓	✓			n/a	n/a	12	7
AVP63-22	✓	✓		✓	n/a	n/a	4	7
AVP63-23		✓			n/a	n/a	12	3

DD   LD

Day 1

Day 2

Figure S1

Figure S2

A

B

C

Rhythmic
Arrhythmic

Rhythmic
Arrhythmic

D

Figure S3

A Intensity

B Events

C Ca Waves

D Ca Wave Duration

E Ca Wave IEI

F

G Intensity

H Acute Events

I Calcium Wave Number
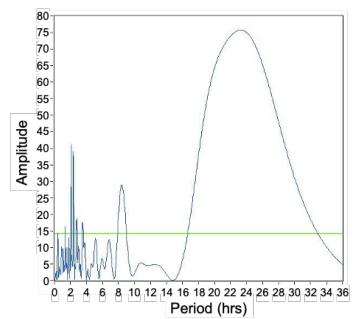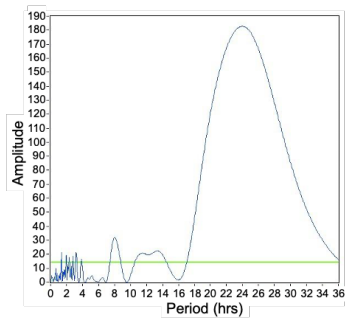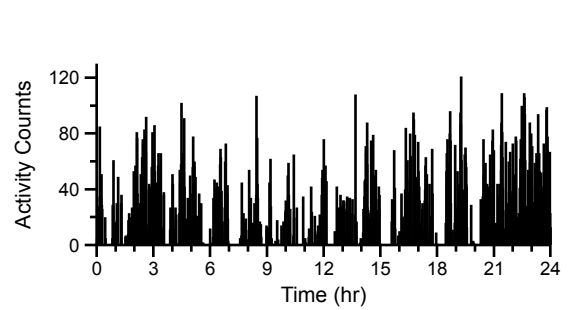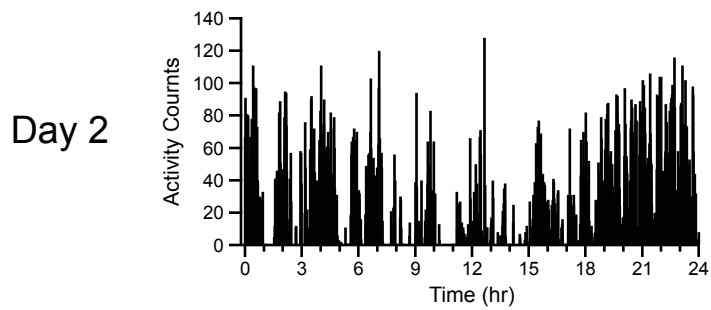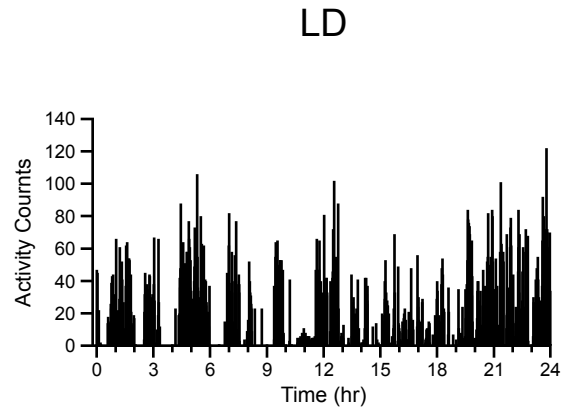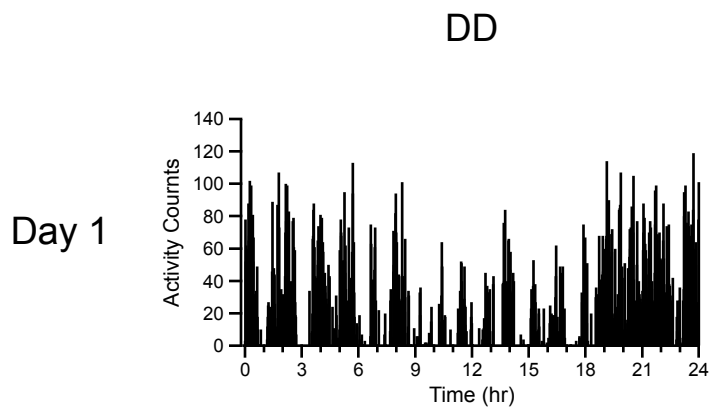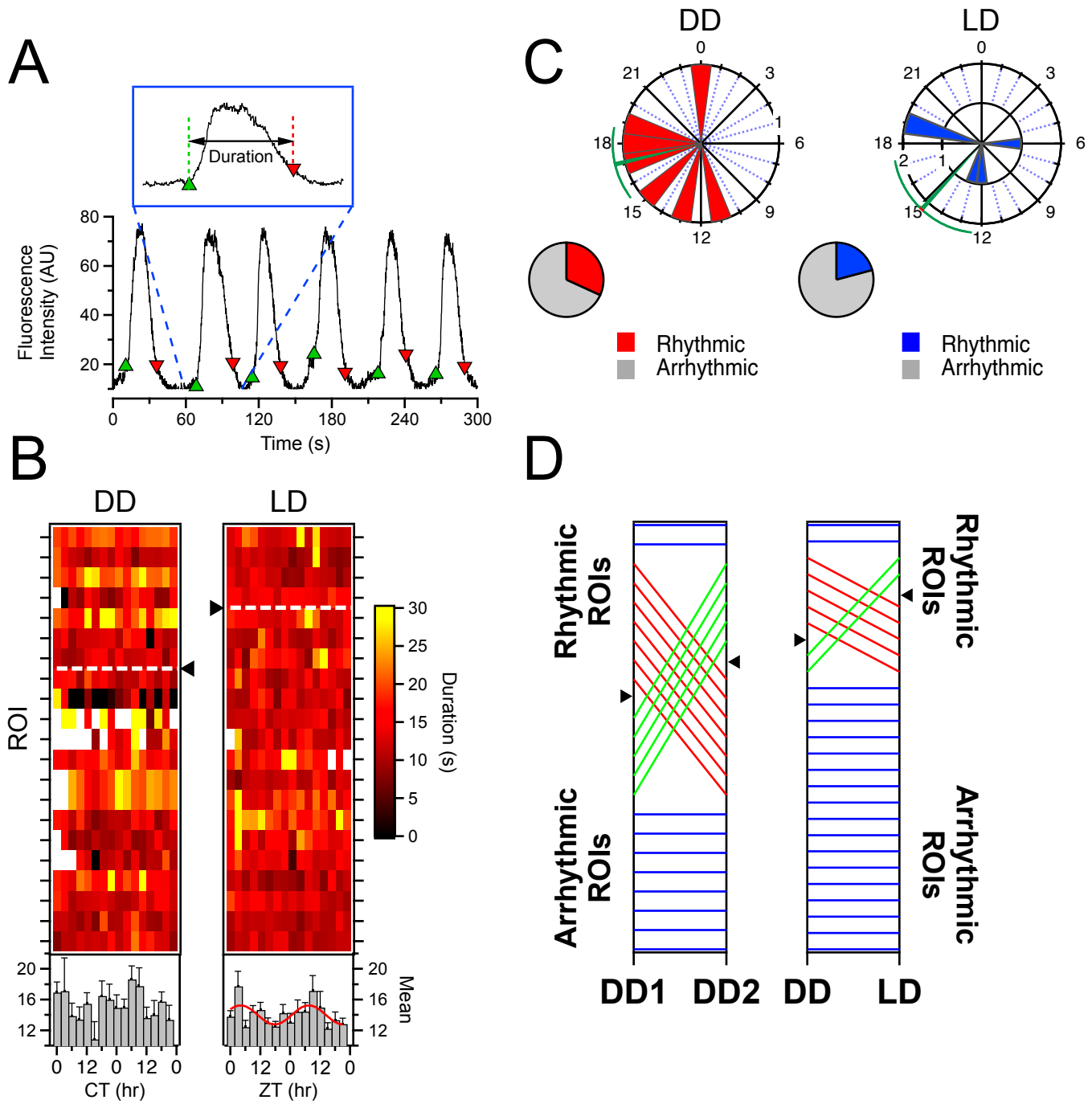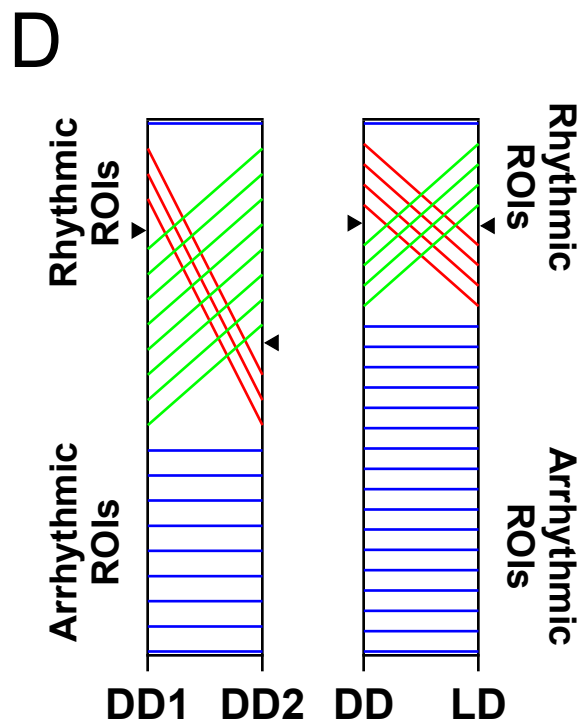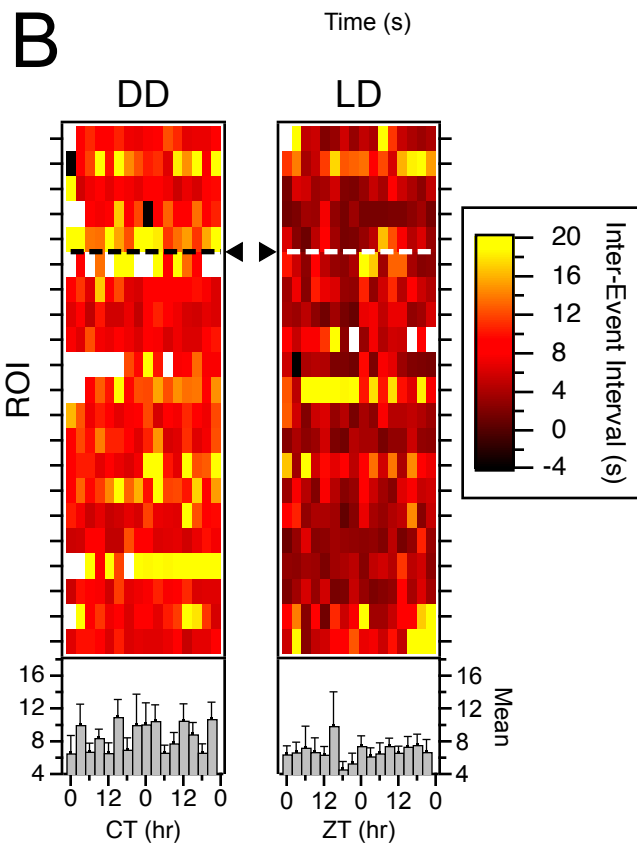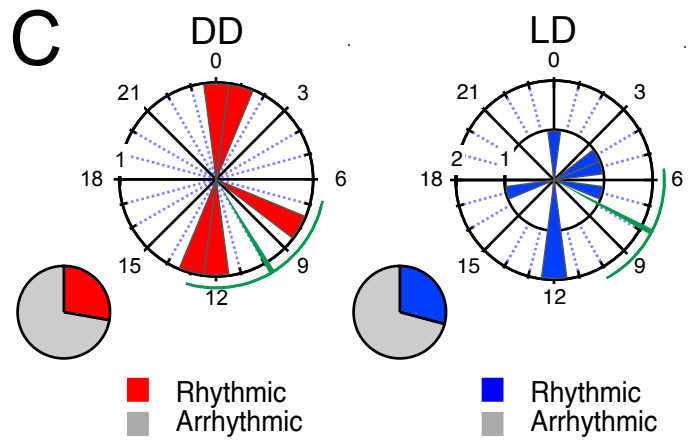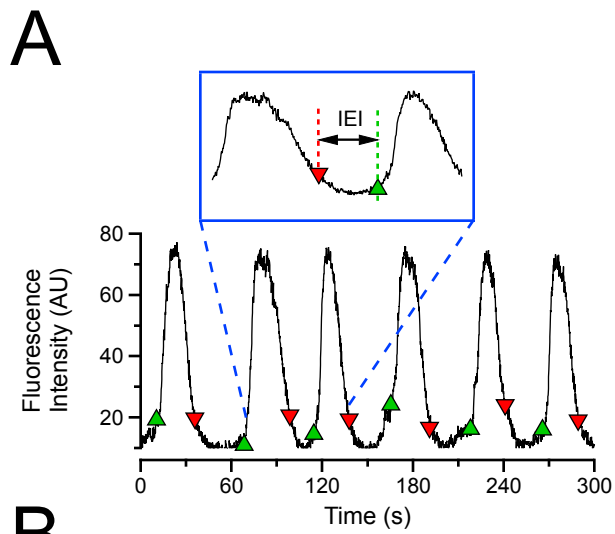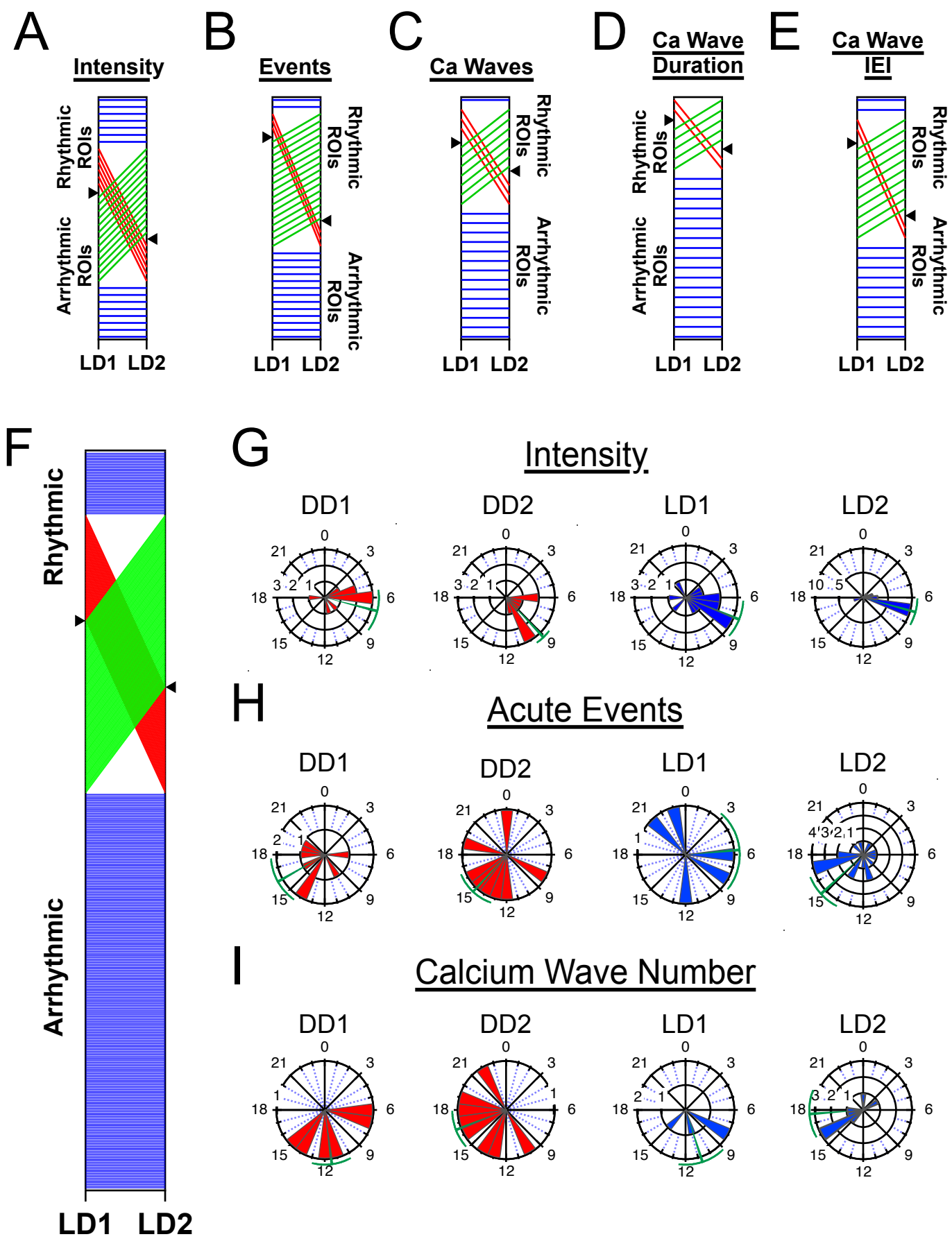
Figure S4

A   Correlations

DD1   DD2   LD1   LD2

B   Calcium Wave Duration

DD1   DD2   LD1   LD2

C   Calcium Wave IEI

DD1   DD2   LD1   LD2
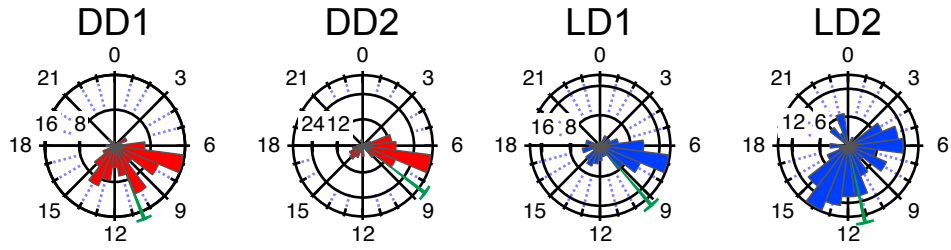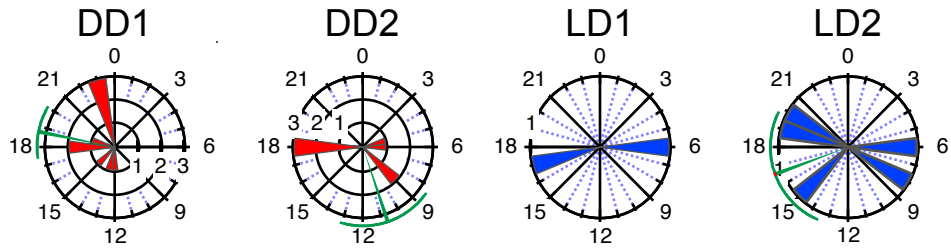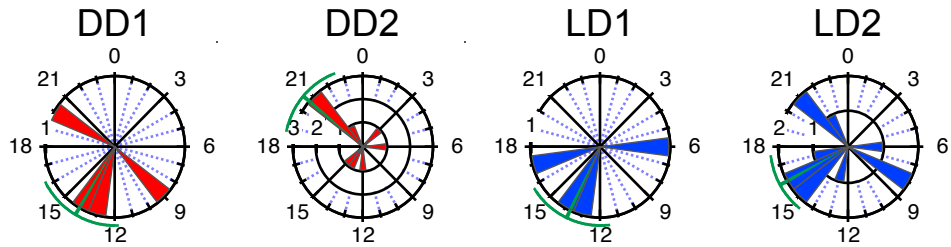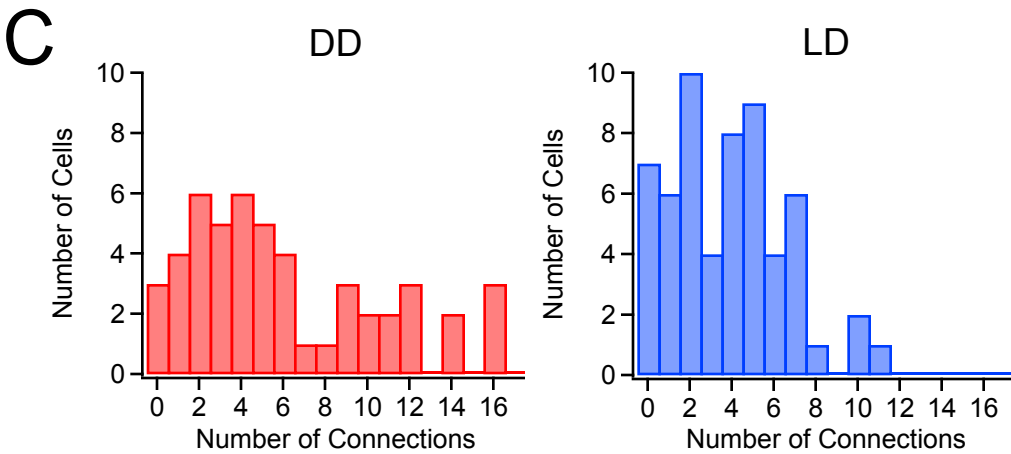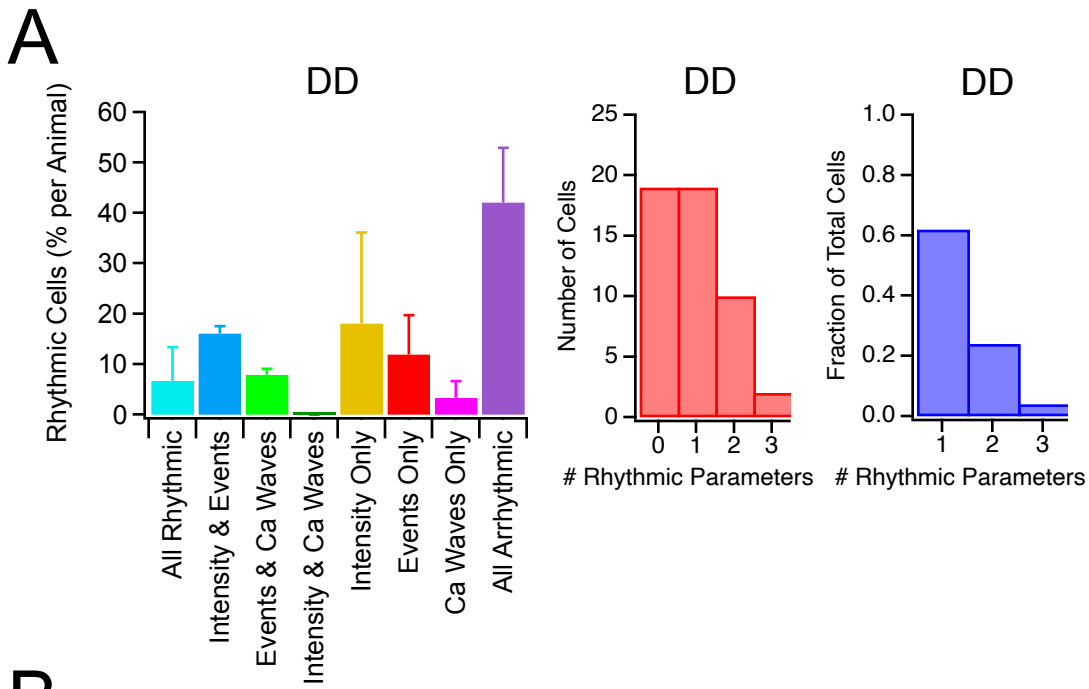
Figure S5

Figure S6

Bootstrapping Intensities

DD

LD

Bootstrap Trial

Bootstrap Trial

0 12 0 12
CT (Hr)

0 12 0 12
ZT (Hr)

Ave Normalized Intensity

5.0
4.5
4.0
3.5
3.0
2.5
2.0
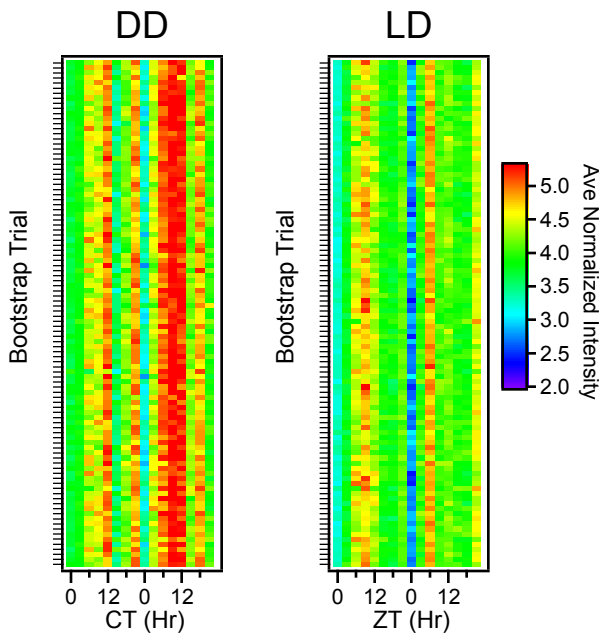
10 ROIs chosen
per animal per trial

Bootstrapping Acute Events

DD

LD

Bootstrap Trial

Bootstrap Trial

0 12 0 12
CT (Hr)

0 12 0 12
ZT (Hr)

Ave Number of Acute Events

17
16
15
14
13
12
11
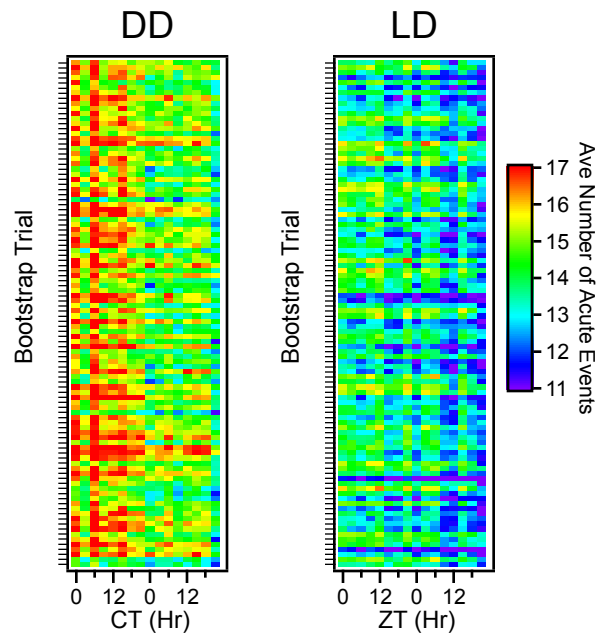
10 ROIs chosen
per animal per trial

Bootstrapping Calcium Waves

DD

LD

Bootstrap Trial

Bootstrap Trial

0 12 0 12
CT (Hr)
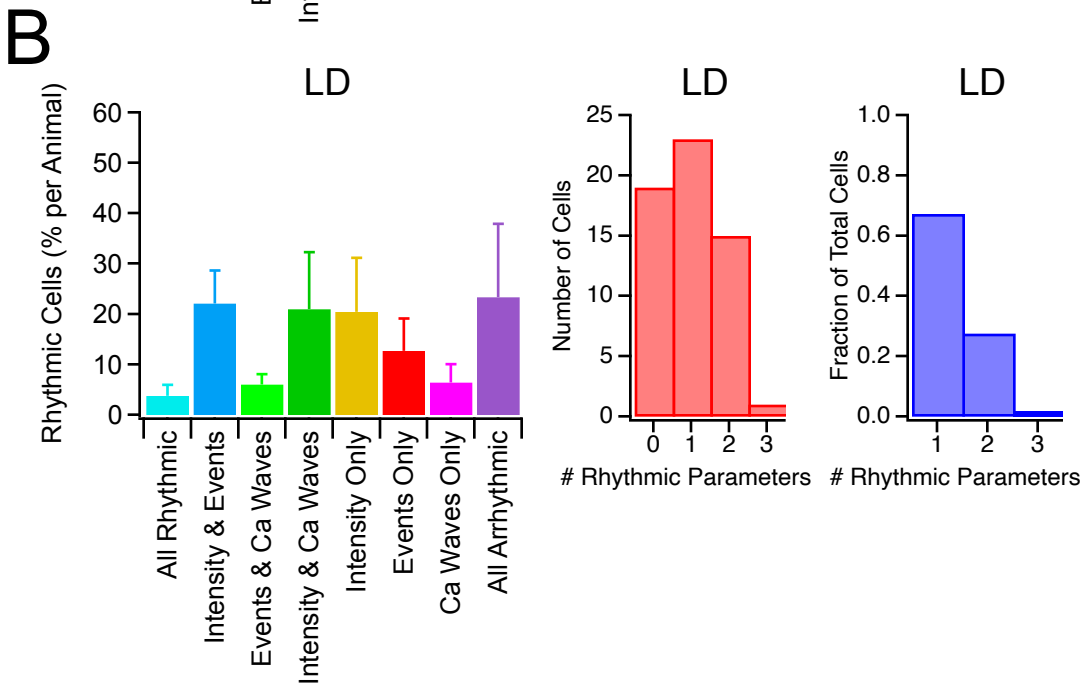
0 12 0 12
ZT (Hr)

Ave Number of Ca Waves

8
7
6
5
4
3
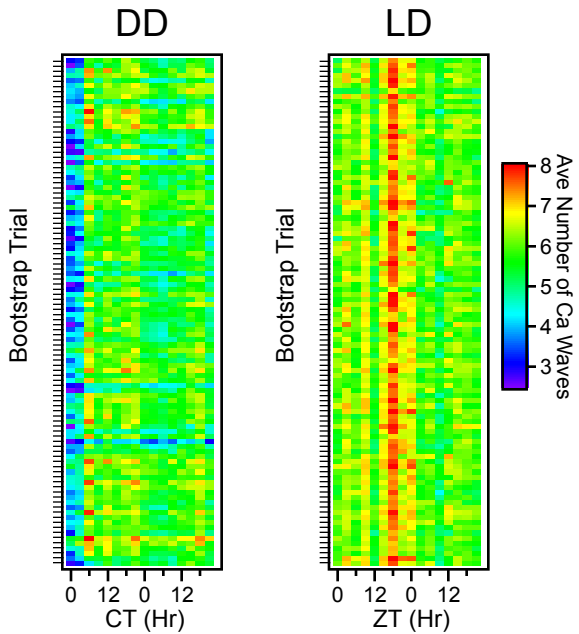
10 ROIs chosen
per animal per trial

Bootstrapping Correlations

DD

LD

Bootstrap Trial

Bootstrap Trial

0 12 0 12
CT (Hr)

0 12 0 12
ZT (Hr)

Ave Pearson Coefficient

0.4
0.3
0.2
0.1
0.0
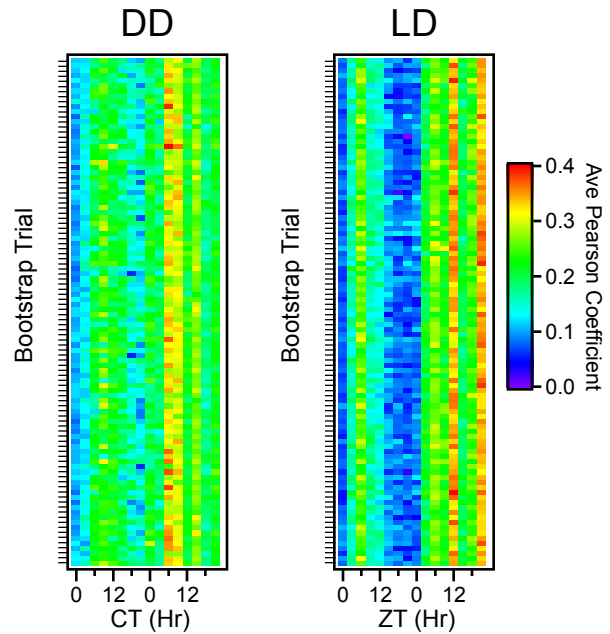
28 ROIs chosen
per animal per trial

Figure S7

Table S2: Bootstrapping Parameters/Results

	Condition	Animal	ROIs Analyzed	Bootstraps per Animal	Trials with p Values < 0.05 (%)
Intensity	DD	AVP24	15	5	57
		AVP44	11	10	69
		AVP63	24	20	77
	LD	AVP10	8	5	73
		AVP24	15	10	91
		AVP44	11	15	93
		AVP63	24		
Acute Events	DD	AVP24	15	5	23
		AVP44	11	10	8
		AVP63	24	20	2
	LD	AVP10	8	5	21
		AVP24	15	10	6
		AVP44	11	20	2
		AVP63	24		
Calcium Waves	DD	AVP24	12	5	38
				10	41
		AVP44	10	20	28
	LD	AVP10	3	5	26
		AVP24	11	10	30
		AVP44	11	20	26

	Condition	Animal	Interactions Analyzed	Bootstraps per Animal	Trials with p Values < 0.05 (%)
Correlations	DD	AVP24	105	28	70
		AVP44	55	55	90
		AVP63	276	105	93
	LD	AVP10	28	14	26
		AVP24	105	28	21
		AVP44	55	55	9
		AVP63	276		

SUPPLEMENTAL METHODS

Image Analysis and Statistics

<u>Image Correction, ROI Definition and Production of Intensity Traces</u>

Raw image stacks acquired at 6.67 Hz were motion-corrected using Inscopix Data Processing software and five-minute recordings of images were exported as TIFF stacks. The TIFF stacks were imported into Igor Pro 8 (Wavemetrics Inc, Lake Oswego, Oregon) for further analysis. For each TIFF stack, a maximum projection image was then produced by finding the maximum intensity for each pixel during the 5-minute recording. This maximum projection image was used to identify regions of interest (ROIs) and regions of background. For a particular animal, ROI locations could vary slightly over the 24 – 48 hours of experimentation, and thus, ROI locations could be slightly corrected from 3-hour time point to time point. Background was subtracted from each image in the stack by doing a two-dimensional interpolation of background intensities based on the background regions outlined in the maximum projection image. Using the background subtracted image stack, the average intensity for each ROI was determined for each image in the stack. This produced a line trace of varying intensities with time over the five-minute period for each ROI (e.g., **Figure 1F-H**).

<u>Mean Intensity, Intensity Correlation and Events Analysis</u>

One focus of this study was to determine if activity of individual neurons varied with circadian rhythmicity. Thus, we characterized each ROI for its average intensity within the five-minute trace at each 3-hour time point (**Figure 1F, Figure 2A-C**). Fluorescence intensity traces for each ROI were also cross-correlated with each other yielding a Pearson coefficient for each ROI-ROI interaction at each circadian time point (**Figure 4A**). We wished to determine if the power in the cross-correlations mainly resulted from slow frequencies below 1 Hz or faster frequencies. To do this, we subjected raw data to high or low pass digital Finite Impulse Response filters before cross-correlation analysis. Parameters for the low pass filter were as follows- End Band Pass: 0.25 Hz; Start of Stop Band: 0.5 Hz; Number of Computed Terms: 73. Parameters of high pass filtering were as follows- End of First Band: 0.5 Hz; Start of Second Band: 1 Hz; Number of terms: 41. Edge effects were removed by deleting the first 17 and last 17 points in the filtered data trace. After cross-correlation analysis, the resulting Pearson Coefficients were analyzed by determining the weights that each of correlation of the filtered traces would contribute to the correlation coefficient that was not digitally filtered:

$$P_{unfiltered} = w_{low\ pass}P_{low\ pass} + w_{high\ pass}P_{high\ pass} \qquad [1]$$

where *P* represents the Pearson Coefficient determined for unfiltered data or for the Pearson Coefficient after filtering the data with either high or low pass filters. *w* represents the contributing weights of each Pearson Coefficient to the Pearson Coefficient determined for the unfiltered data. An additional constraint was that:

$$w_{low\ pass} + w_{high\ pass} = 1$$

In addition, we performed event analysis on the calcium traces. This was accomplished in two different ways. An unbiased analysis of acute events was conducted in which the

onset of an event was found if the amplitude increased by more than two standard deviations above the intensity of the previous 20 points (3 seconds) (**Figure 1G, Figure 2 D-F**). Data was smoothed prior to this analysis using a 30-point box window. A second method was used to determine event parameters of slow calcium waves (**Figure 1H, Figure 2 G-I**). In a first pass, automatic analysis was done in which the raw fluorescence line trace for each ROI was smoothed with a 50-point box window. Then, the first derivative was calculated from the smoothed raw data trace. The first derivative trace was also smoothed using a 100-point box window followed by recording the time when a threshold level on the first derivative was crossed in an increasing manner when searching from the start of the first derivative trace to the end for either positive or negative slopes. This approximated the start of slow calcium fluorescence wave rise and the end of the calcium wave. The value of the threshold of the first derivative was determined heuristically (usually 0.05). These time points could then be manually corrected for missing and/or spurious events. Wave durations, inter-event intervals and wave number could then be calculated from the start and end times of each event in each fluorescent intensity line trace.

Circadian Rhythm Analysis

Circadian Rhythmicity was tested by fitting data collected at three-hour intervals over 24 or 48 hours with a cosine function as follows:

$$y = \frac{A}{2}\cos\left(\frac{2\pi(t-\psi)}{\theta}\right) + \frac{A}{2} + A_o \qquad [2]$$

where A represents the amplitude of the cosine signal, A_o is the average offset of the fluorescence signal from zero, t is the time of each data point in hours, ψ and θ are the phase and period respectively in hours resulting from the fit. The data that were fit with Equation 2 to determine rhythmicity were the mean intensities, intensity correlations between ROIs, the wave number for dynamic calcium events as well as the number of calcium waves. Before fitting mean intensities, data was subjected to linear detrending to compensate for any consistent, progressive loss of fluorescence intensity over the period of the experiment. Fit optimization was performed using the internal Igor Pro algorithm based on Levenberg-Marquardt least-squares method constraining the results for the period between 20 and 32 hours. The p-values from these fits were determined using the Igor Pro implementation of the non-parametric Mann-Kendall tau test. A measure for a particular ROI was deemed rhythmic if the p-value was below 0.05. The 24- or 48-hour data was then ranked by p-value and displayed as heatmaps. Data which could not be fit with Equation 2 was given a p-value of 1 in the resulting heatmaps and is not ranked (**Figures 2A, 2D, 2G, 4B**). Those non-rhythmic ROIs are plotted below the dotted line in each heatmap.

To determine if AVP neurons displayed any rhythmicity as a population, the columns of the heatmaps were averaged, and these values subject to the circadian fit using Equation 2. For population averages, fitting was also weighted by the reciprocal of the standard deviations determined for each column of the heatmap. When the population measure was rhythmic, the cosine fit is displayed on the mean bar graph below each heat map (**Figures 2A, 2D, 2G, 4B**).

Phases (ψ) resulting from the fits to Equation 2 were saved for each ROI or ROI-ROI interaction with significant rhythmicity. Histograms of the phases were then calculated utilizing 3-hour bins and then plotted on polar coordinate graphs (**Figures 2B, 2E, 2H and 4C**).

<u>Bootstrapping analysis for population-level rhythmicity</u>

In our study, the number of GCaMP7 fluorescent neurons found in each animal varied from 8 to 24 neurons. Thus, it is possible that each of the mice examined in our study may have an unequal contribution to the population rhythm for each measure (straight averages of all cells are shown below each heatmap in Figures 2A, 2D, 2G and 4B). For this reason, we have run a bootstrapping protocol on the data, where each animal only supplies an equal number of cells to the analysis. The overall workflow follows the heatmap analysis to determine if a population rhythm existed and is as follows. Data from heatmaps in Figures 2A, 2D, 2G and 4B were divided up per animal. The number of rows to be used per animal was chosen (**Table S2**), thus equalizing the contribution of each mouse. As in the original analysis, each row contained 16 measurements taken every 3 hours over a 48-hour period. Then, a random number generator was used to determine which rows (ROIs for Intensity, Acute Events and Calcium Waves or ROI-ROI cross-correlations for Correlations) from each animal would be chosen to contribute to the population measurement. After these data were chosen for each mouse, the columns representing each time point were then averaged to yield a population measurement for each time point. This was considered one complete bootstrapped experiment. Each bootstrap experiment was run 100 times and the heatmaps found in Figure S7 show the results, where each row represents the average population measurement of a single bootstrap experiment. As with the original data, each bootstrap trial (1 row in heatmaps in **Figure S7**) was checked for rhythmicity by subjecting each row to a cosinor fit and Mann-Kendall statistical test. The number of population measurements which gave a $p < 0.05$ was then reported in the last column of **Table S2**. This procedure was run several times for the different data sets, inputting different numbers of ROIs/cross-correlations to be tested per animal (Table 2). In some cases, where less data for an individual animal was available, oversampling was done.

<u>Calculation of Firing Rate and Duration of Bursting for Single Unit Analysis</u>

After spike sorting, traces dedicated to a particular single unit were analyzed for their firing rate (**Figure 3E**). Time stamps of action potential firing were subjected to histogram analysis with a bin size of 3 s for over the whole recording and then divided by the bin size to get the firing rate per 3 s time point. A histogram of this firing rate time course was then made, indicating the prevalence of firing rates. Burst lengths were determined by rebinning the time stamp data per 10 s bins and determining the duration of the burst by analyzing the points when the firing rate had risen above and then returned below 1.5 Hz (**Figure 3G**). 1.5 Hz was determined empirically, as it seemed to correlate with bursting behavior observed by eye. Because firing rates and burst lengths could have a range of several decades, these histograms were converted to a log transform where the abscissa was the log of the firing rate and the ordinate was the square root of the number of events per bin (e.g. **Figures 3G**, **3H**). This data was then fit with a log transformation of a sum of exponential components using the following equation[50]:

$$y = A_0 + \sum_i^n \left(\frac{A_i}{\tau_i} e^{\left(t - \frac{e^t}{\tau_i} \right)} \right) \qquad\qquad [3]$$

where A_i is the amplitude of the exponential of component i, A_0 is the amplitude offset, τ_i is the exponential time constant of component i and n is the number of exponentials in the log transform. The variable t is the firing rate or the burst length for **Figures 3G** and **3H**, respectively.